




# Zwitterionic Granular Hydrogel for Cartilage Tissue Engineering

## Journal Article

### Author(s):

[Asadikorayem, Maryam](#) ; [Surman, František](#); [Weber, Patrick](#) ; [Weber, Daniel](#); [Zenobi-Wong, Marcy](#) 

### Publication date:

2023

### Permanent link:

<https://doi.org/10.3929/ethz-b-000629721>

### Rights / license:

[Creative Commons Attribution-NonCommercial 4.0 International](#)

### Originally published in:

Advanced Healthcare Materials, <https://doi.org/10.1002/adhm.202301831>

### Funding acknowledgement:

192656 - Zwitterionic Materials for Treatment of Osteoarthritis (SNF)

# Zwitterionic Granular Hydrogel for Cartilage Tissue Engineering

Maryam Asadikorayem, František Surman, Patrick Weber, Daniel Weber, and Marcy Zenobi-Wong\*

Zwitterionic hydrogels have high potential for cartilage tissue engineering due to their ultra-hydrophilicity, nonimmunogenicity, and superior antifouling properties. However, their application in this field has been limited so far, due to the lack of injectable zwitterionic hydrogels that allow for encapsulation of cells in a biocompatible manner. Herein, a novel strategy is developed to engineer cartilage employing zwitterionic granular hydrogels that are injectable, self-healing, in situ crosslinkable and allow for direct encapsulation of cells with biocompatibility. The granular hydrogel is produced by mechanical fragmentation of bulk photocrosslinked hydrogels made of zwitterionic carboxybetaine acrylamide (CBAA), or a mixture of CBAA and zwitterionic sulfobetaine methacrylate (SBMA). The produced microgels are enzymatically crosslinkable using horseradish peroxidase, to quickly stabilize the construct, resulting in a microporous hydrogel. Encapsulated human primary chondrocytes are highly viable and able to proliferate, migrate, and produce cartilaginous extracellular matrix (ECM) in the zwitterionic granular hydrogel. It is also shown that by increasing hydrogel porosity and incorporation of SBMA, cell proliferation and ECM secretion are further improved. This strategy is a simple and scalable method, which has high potential for expanding the versatility and application of zwitterionic hydrogels for diverse tissue engineering applications.

(OA), due to their lack of intrinsic tissue healing capacity. Numerous tissue engineering strategies have been reported to treat focal cartilage lesions by combining cells, biomaterials, and advanced biofabrication techniques.<sup>[1]</sup> Intra-articular delivery of cells embedded in supportive injectable hydrogels, is one of the most promising noninvasive approaches for treating large cartilage defects.<sup>[2]</sup> Although major advances have been made in optimizing cell sources, crosslinking strategies, and biofabrication techniques, designing of a perfectly biocompatible and nonimmunogenic biomaterial for cartilage tissue engineering applications is still an unmet challenge.<sup>[3]</sup>

Even though articular cartilage is generally regarded as an immune-privileged tissue, this is not the case for injured or osteoarthritic cartilage.<sup>[4]</sup> In traumatic osteochondral defects or through most repairing operations, bone marrow, or synovium tissue-residing immune cells can infiltrate the tissue as well as the implanted construct and elicit an immune reaction.<sup>[5]</sup> Also, the biomaterial itself can induce local tissue inflammation and

immune response.<sup>[6]</sup> Such immune reactions can disturb tissue regeneration processes and result in implant failure. Flégeau et al. recently showed that cell-laden hydrogels based on hyaluronic acid are fully infiltrated by host immune cells six weeks after subcutaneous implantation in vivo in nude rats, resulting in implant degradation and impaired stability of the construct.<sup>[7]</sup> Therefore, successful cartilage tissue regeneration requires that the interaction of the biomaterial with immune cells is carefully considered to avoid exacerbating existing inflammation.<sup>[8]</sup>

Among the plentiful natural and synthetic polymers used in tissue engineering, zwitterionic materials have gained particular attention because of their superior antifibrotic and nonimmunogenic properties.<sup>[9]</sup> Zwitterions have equal number of anionic and cationic groups in close spatial proximity, which results in high levels of hydration, giving them nonfouling properties and high biocompatibility.<sup>[10]</sup> Several studies have demonstrated that hydrogels made of zwitterionic polymers can effectively resist foreign body reaction and collagen capsule formation in immunocompetent animals up to one year after implantation.<sup>[9,11]</sup> Zwitterionic hydrogels have also been shown to maintain multipotency

## 1. Introduction

Articular cartilage lesions, if not treated, put a relatively young and healthy population on the path to degenerative osteoarthritis

M. Asadikorayem, F. Surman, P. Weber, M. Zenobi-Wong  
Tissue Engineering + Biofabrication Laboratory  
Department of Health Sciences and Technology  
ETH Zürich, Otto-Stern-Weg 7, Zürich 8093, Switzerland  
E-mail: marcy.zenobi@hest.ethz.ch

D. Weber  
Division of Hand Surgery  
University Children's Hospital  
Zürich 8032, Switzerland

 The ORCID identification number(s) for the author(s) of this article can be found under <https://doi.org/10.1002/adhm.202301831>

© 2023 The Authors. Advanced Healthcare Materials published by Wiley-VCH GmbH. This is an open access article under the terms of the Creative Commons Attribution-NonCommercial License, which permits use, distribution and reproduction in any medium, provided the original work is properly cited and is not used for commercial purposes.

DOI: 10.1002/adhm.202301831

and avoid nonspecific differentiation of mesenchymal stem cells,<sup>[12]</sup> and significantly promote ex vivo culture of human hematopoietic stem and progenitor cells due to their reactive oxygen species scavenging properties.<sup>[13]</sup>

We believe that zwitterionic hydrogels with their nonimmunogenicity and antifouling properties are an excellent choice for cartilage tissue engineering, to provide optimal environment for tissue regeneration by minimizing any disturbing immunological response. However, their application in cartilage tissue engineering has been limited so far. Zwitterionic microspheres have been used for cartilage tissue regeneration, due to their unique lubrication properties.<sup>[14]</sup> Also, zwitterionic hydrogels have shown immunomodulatory effect on chondrocytes cultured in inflammatory media in vitro and therapeutic effect toward osteoarthritis in vivo.<sup>[15]</sup> However, an injectable zwitterionic hydrogel which allows for direct encapsulation of chondrocytes and supports chondrogenesis and extracellular matrix (ECM) production has not been introduced yet.

Zwitterionic polymer solutions have normally very low viscosities, making them not suitable for injectable formulations. To provide injectability as well as versatility, we have designed zwitterionic granular hydrogels as opposed to conventional bulk hydrogels. Granular hydrogels are fabricated by chemical annealing or physical jamming of hydrogel microparticles called microgels.<sup>[16]</sup> They have inherent injectability due to microgel's ability to flow under shear force and microporosity through microgel packing.<sup>[17]</sup> Granular hydrogels have been demonstrated to support higher cell proliferation and migration compared to the bulk hydrogels in vitro.<sup>[18]</sup> It has also been shown in several studies that encapsulation of cells in granular hydrogels results in improved hyaline cartilage formation in cartilage defect models in vivo.<sup>[19]</sup> Moreover, granular hydrogels can provide physical protection to cells during the injection process from high levels of fluidic shear stress.<sup>[20]</sup>

Thus, the goal of this study is to design a zwitterionic granular hydrogel for cartilage tissue engineering that combines injectability and microporosity of granular hydrogels with biocompatibility and nonimmunogenicity of zwitterionic materials. First, zwitterionic microgels are produced with mechanical fragmentation of the photocrosslinked bulk hydrogels made of zwitterionic carboxybetaine acrylamide (CBAA) monomer or a mixture of CBAA and zwitterionic sulfobetaine methacrylate (SBMA), using gelatin methacryloyl (GelMA) as a biocompatible crosslinker. SBMA was incorporated because it has been previously shown that it supports cell attachment more than other zwitterionic hydrogels.<sup>[21]</sup> Thus, we hypothesized that incorporation of SBMA would enhance chondrogenic potential of the zwitterionic CBAA hydrogels. The resulting microgels were then mixed with cells and secondarily crosslinked using horseradish peroxidase (HRP) and hydrogen peroxide ( $H_2O_2$ ) resulting in a microporous scaffold, which is stable in aqueous media, with cells residing in the pores between microgels (**Figure 1**). To realize secondary crosslinking of microgels, we synthesized tyramine acrylamide (TyrAA) comonomer, which is incorporated in the bulk zwitterionic hydrogel through photopolymerization process. The tyramine moieties can then be exploited for secondary crosslinking of the microgels in the presence of crosslinkers and cells in a cytocompatible and in situ crosslinkable manner. Rheological and mechanical properties of the zwitterionic granular

hydrogels with different microgel sizes were characterized. Also, primary human chondrocytes were encapsulated in these granular hydrogels to study their potential for chondrogenesis and cartilage tissue engineering. Overall, this study introduces a simple, scalable, and yet versatile method to produce zwitterionic granular hydrogels that are injectable, allow for direct cell encapsulation, undergo enzymatic secondary crosslinking to immediately stabilize the construct and can be used for diverse tissue engineering applications.

## 2. Results and Discussion

### 2.1. Production of Zwitterionic Granular Hydrogels with Tunable Porosity

Transplant failure caused by low biocompatibility and immunogenicity of biomaterials is a challenge in cartilage tissue engineering and defect repair.<sup>[22]</sup> In cartilage defects, the joint environment is inflamed with immune cells from bone and synovium tissue invading the defect and resulting in tissue degradation and inhibited healing due to secretion of inflammatory proteases.<sup>[5b]</sup> Exacerbated inflammation due to immunogenicity of the biomaterials used for defect repair, can result in further degradation and impaired healing.<sup>[23]</sup> As there is a large body of literature showing nonimmunogenicity and in vivo biocompatibility of zwitterionic materials, we opted to develop a versatile zwitterionic hydrogel for cartilage defect repair in this study. Zwitterionic materials with their exceptional biocompatibility, can provide an optimal environment for delivered cells in vivo to effectively regenerate the defect. Zwitterionic CBAA monomer was used to produce zwitterionic granular hydrogels. Among diverse zwitterionic monomers, it has been shown that CBAA hydrogels possess a higher degree of hydration and tighter interactions with water molecules,<sup>[24]</sup> making them the most antifouling hydrogels. Also, CBAA monomer has one carboxylate pendant group, which can be used for further functionalization and incorporation of amine-containing biomolecules.<sup>[25]</sup> Due to its versatile functionalization and nonfouling properties, CBAA is particularly desirable for biomedical applications and can be an excellent alternative to polyethylene glycol (PEG), a commonly used synthetic polymer. In comparison to CBAA, PEG has several disadvantages including susceptibility to oxidation and production of anti-PEG antibodies.<sup>[10,26]</sup>

First, CBAA monomer and TyrAA comonomer were synthesized as shown in Figure S1 of the Supporting Information. Successful and high purity synthesis was confirmed with  $^1H$  NMR for both monomers (Figures S2 and S3, Supporting Information). GelMA with DS  $\approx$  73%, as calculated from  $^1H$  NMR, was also synthesized to be used as crosslinker for bulk hydrogel production. We used GelMA as crosslinker as it is biocompatible and also provides cell-binding sites.<sup>[27]</sup> Bulk zwitterionic hydrogel was produced by free radical photopolymerization of aqueous solution of CBAA and TyrAA comonomer with GelMA and lithium phenyl-2,4,6-trimethylbenzoylphosphinate (LAP) as photoinitiator using UV-vis (405 nm) irradiation. The bulk hydrogel was extensively dialyzed to remove unreacted monomer and photoinitiator and also to reach equilibrium swelling. The hydrogel was highly swollen with equilibrium water content (EWC) reaching 93–94% and quite soft with a compressive modulus of  $\approx$ 6 kPa.

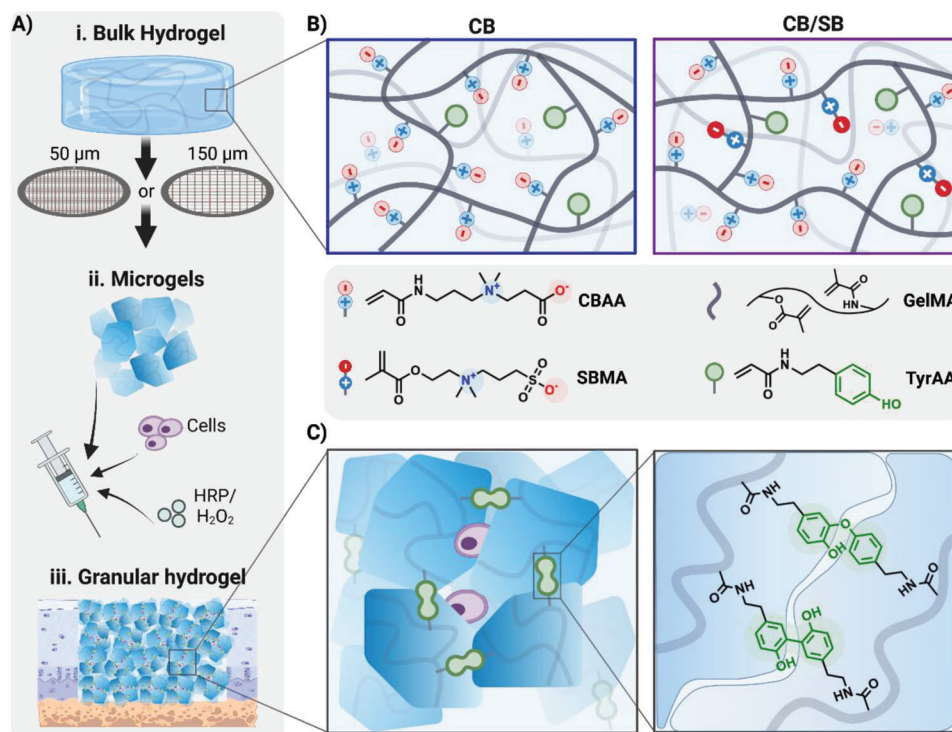


**Figure 1.** Illustration of zwitterionic granular hydrogel for cartilage tissue engineering. A) Zwitterionic bulk hydrogel is mechanically fragmented to produce zwitterionic microgels using  $\mu\text{m}$ -sized grids, microgels are mixed with cells and crosslinkers (HRP and  $\text{H}_2\text{O}_2$ ) resulting in an injectable formulation that can be injected into cartilage defect and crosslinked in situ resulting in zwitterionic granular hydrogel. B) Bulk hydrogel structure made of either pure CBAA (CB) or a mixture of CBAA and SBMA (CB/SB) crosslinked with GelMA and incorporating the functional comonomer, TyrAA, which is required for secondary crosslinking. C) Secondary crosslinking of microgels with covalent bond formation between phenol groups of TyrAA comonomer in presence of HRP and  $\text{H}_2\text{O}_2$  resulting in microporous granular hydrogel encapsulating cells.

The swelling and mechanical properties of the bulk hydrogel are shown in Figure S4 of the Supporting Information.

Microgels can be produced either by processing a hydrogel precursor into droplets before crosslinking or by fragmenting crosslinked bulk hydrogels into smaller particles. Droplets can be formed by different methods such as batch emulsion,<sup>[28]</sup> coacervation,<sup>[29]</sup> particle replication in nonwetting templates (PRINTs),<sup>[30]</sup> and microfluidics.<sup>[31]</sup> Techniques such as PRINT and microfluidics offer high control over droplet shape and size; however, these techniques are complicated, have a low yield, and are not easy to scale.<sup>[32]</sup> We used mechanical fragmentation for granular hydrogel fabrication,<sup>[33]</sup> as it is a simple and scalable method, does not require the use of any toxic materials, and the average microgel size and porosity can be easily controlled by changing the mesh size. Moreover, the resulting granular hydrogel supports long-term cell culture, as it has higher mechanical stability compared to other microgel fabrication techniques, thus suiting our application.<sup>[34]</sup>

Bulk hydrogels were mechanically pressed through  $\mu\text{m}$ -sized metal grids using a custom-made extruder. We used two different grids with 50 or 150  $\mu\text{m}$  aperture diameter to have two different sets of granular hydrogels with different microgel sizes and thus different porosities. After mechanical fragmentation, microgels were immersed in ethanol for sterilization, dried, and then reswollen in aqueous buffer. Dried microgels can also be stored at this step for later use.

As shown in **Figure 2A**, the resulting zwitterionic microgel is perfectly injectable; however, these microgels are quickly dispersed in aqueous media after injection (**Figure 2B**). This is because the weak physical and frictional interactions between microgels is not enough to hold them together, resulting in suboptimal mechanical stability and integrity and lack of stability in aqueous media. This can be particularly problematic if granular hydrogels are used to deliver cells or other bioactive molecules in vivo, as this can lead to insufficient retention of the cargo in the body and no targeted delivery. To produce stable granular hydrogels, dried microgels were swollen in PBS as 6 wt%, matching the  $\approx 94\%$  EWC of the initial bulk hydrogel. Then, secondary crosslinking of the microgels was done by mixing them with HRP and  $\text{H}_2\text{O}_2$ , triggering the crosslinking of Tyr-AA moieties, which were incorporated in the bulk hydrogel production. As shown in **Figure 2B**, crosslinked microgels are stable in aqueous media and do not disintegrate like uncrosslinked microgel's slurry do, indicating successful covalent bond formation between microgels upon enzymatic crosslinking. The crosslinked microgels result in stable, self-supporting scaffolds that can be easily handled with tweezers, and are also stable in aqueous media over time without evident swelling or disintegration (**Figure S5**, Supporting Information).

With the incorporation of fluorescein *o*-acrylate comonomer in bulk hydrogel production, resulting microgels can be visualized and analyzed using a confocal microscope. We used two grid

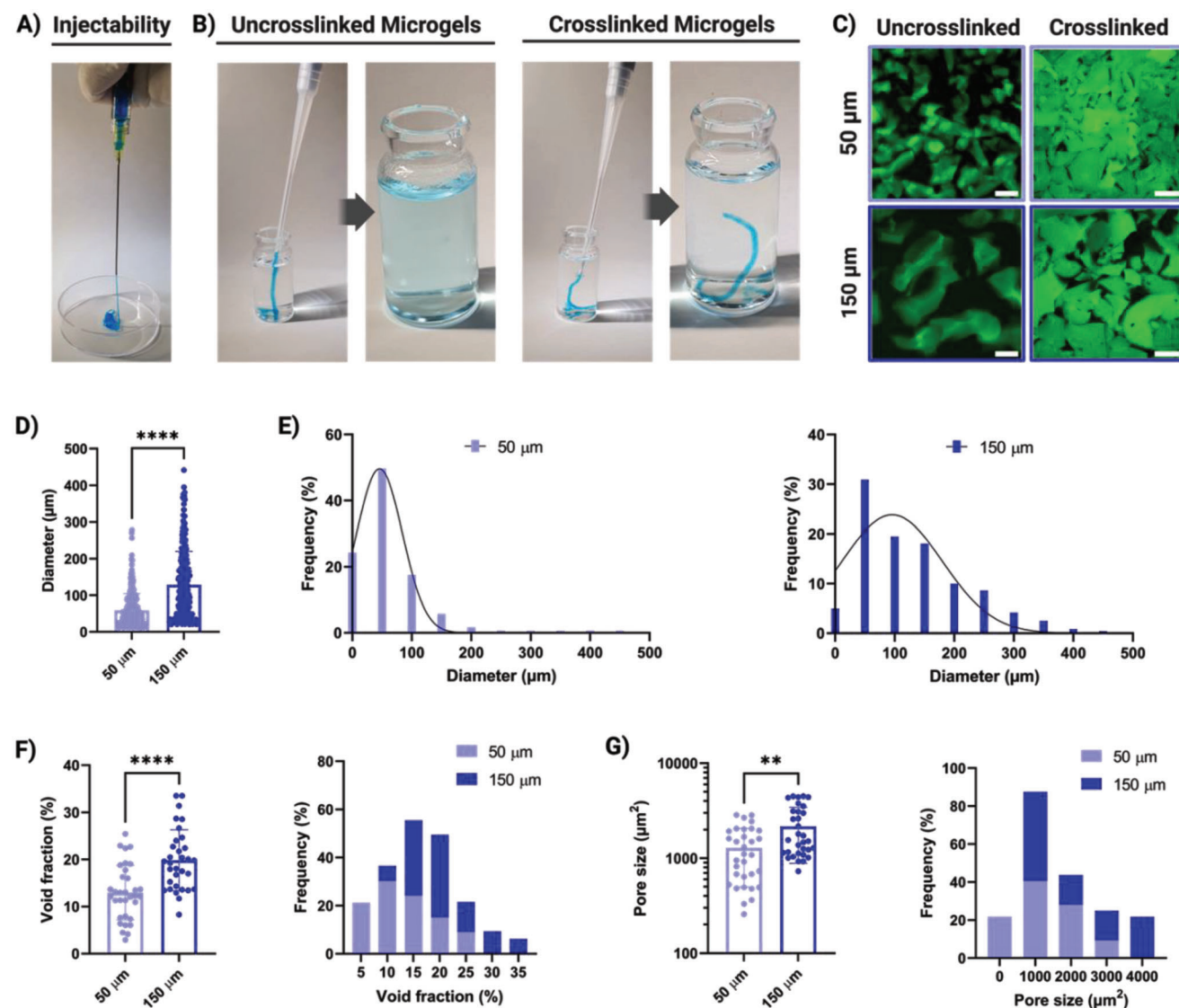


**Figure 2.** Zwitterionic microgels and granular hydrogel characterization. A) Images of zwitterionic microgels injectability. B) Uncrosslinked microgels injected into aqueous media are easily and quickly dispersed and are not stable (left), crosslinked microgels (microgels + HRP and  $\text{H}_2\text{O}_2$ ) injected into aqueous solution are stable and do not disperse (right). C) Confocal images of uncrosslinked and crosslinked microgels made with 50 and 150  $\mu\text{m}$  grids. Fluorescein *o*-acrylate was incorporated into the hydrogel for visualization purposes. Scale bar: 200  $\mu\text{m}$ . D) Average diameter of microgels after sizing ( $n = 300$  individual microgels). E) Size distribution for microgels sized with 50 and 150  $\mu\text{m}$  grid. F) Average void fraction in the crosslinked granular hydrogels (left) and void fraction distribution (right) ( $n = 3$  granular hydrogels, 10 images per hydrogel). G) Average pore size in the crosslinked granular hydrogels (left) and pore size distribution (right) ( $n = 3$  granular hydrogels, 10 images per hydrogel). Data are represented as mean  $\pm$  standard deviation. (D,F,G) Statistical significance was determined using unpaired *t*-test (\*\* $p < 0.01$  and \*\*\*\* $p < 0.0001$ ).

sizes of 50 and 150  $\mu\text{m}$  to study the effect of microgel size on granular hydrogel characteristics. Produced microgels have irregular and polygonal surfaces (Figure 2C), which are characteristics of the microgels from mechanical fragmentation techniques. The granular hydrogels' morphology after enzymatic crosslinking was also evaluated by confocal microscopy (Figure 2C), showing microgel packing and the void space between microgels for both microgel sizes, which are required for optimal cell proliferation and ECM deposition. Using ImageJ, we analyzed confocal images and evaluated individual microgel size. The average di-

ameter for microgels is controlled by the size of the grid used for their fabrication and is  $59 \pm 45 \mu\text{m}$  for the 50  $\mu\text{m}$  grid and  $129 \pm 91 \mu\text{m}$  for the 150  $\mu\text{m}$  grid (Figure 2D). Both microgel groups are polydisperse with wide size distributions, while microgels made with smaller (50  $\mu\text{m}$ ) grid have relatively narrower size distribution (Figure 2E).

Cross-sectional areas occupied by void spaces in fluorescently labeled granular hydrogels were also determined using ImageJ and referred to as void fraction, as an indication of porosity. The size of the individual voids between packed microgels was also

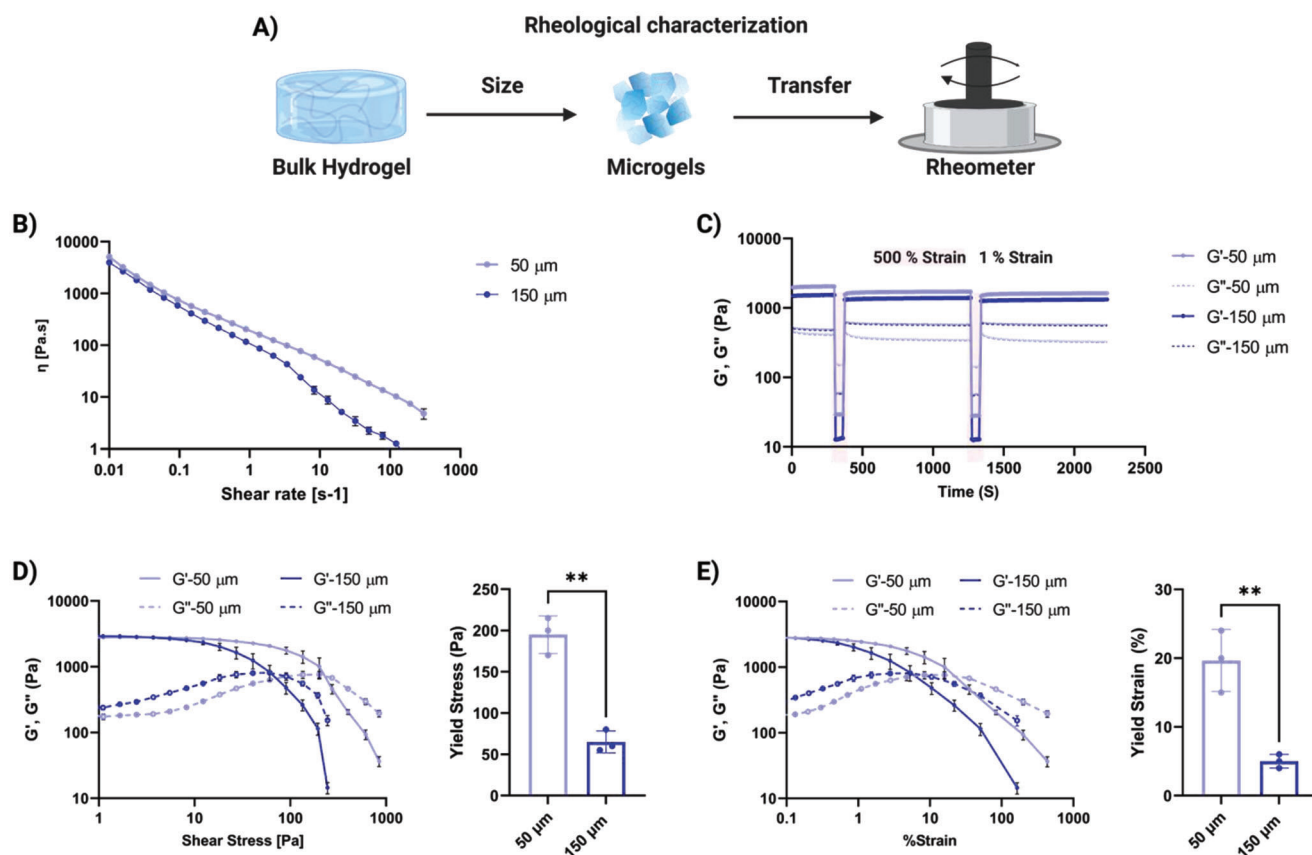


**Figure 3.** Rheological characterization of zwitterionic microgels. A) Schematic of the rheometry workflow. B) Shear-thinning behavior measured by rotational rheometry with ramped shear rate ( $0.01\text{--}300\text{ s}^{-1}$ ). C) Shear-recovery behavior measured by oscillatory rheometry with cycles of low (1%) and high (500%) strain. Stress sweep measured by oscillatory rheometry (1 Hz,  $1\text{--}1000$  Pa, ramp logarithmic) to measure D) yield stress and E) yield strain. Data are represented as mean  $\pm$  standard deviation. (D,E) Statistical significance was determined using unpaired *t*-test (\*\* $p < 0.01$ ) ( $n = 3$  replicates).

analyzed and referred to as pore size. In general, different microgel fabrication techniques result in a diverse range of scaffold porosities. Very high porosities (65–90%) have been reported for high aspect ratio rod-shaped microgels made by the PRINT technique.<sup>[30a]</sup> However, the effect of such high porosity on long-term stability of the samples and the response of the directly encapsulated cells has not yet been studied. Porosities ranging from 2% to 20% have been reported with mechanical fragmentation technique depending on the biomaterial type, microgel size and annealing strategy.<sup>[7,34]</sup> Our zwitterionic granular hydrogels had overall high porosities, with  $13\% \pm 6\%$  total void space for granular hydrogels composed of  $50\ \mu\text{m}$ -sized microgels and  $20\% \pm 6\%$  for  $150\ \mu\text{m}$ -sized microgels (Figure 2F). This is in accordance with the literature stating that decreasing particle size results in reduced porosity.<sup>[29,35]</sup> Furthermore, both granular hydrogels have pores with varying sizes ranging from  $\approx 300$  to  $4000\ \mu\text{m}^2$ , with average pore size controlled by grid size, being smaller for smaller microgels ( $1282 \pm 784$  and  $2167 \pm 1281\ \mu\text{m}^2$  for  $50$  and  $150\ \mu\text{m}$ -grid microgels, respectively) (Figure 2G). In summary, zwitterionic granular hydrogels with differing microgel sizes and porosities were achieved through mechanical fragmentation and enzymatic crosslinking, which are stable in aqueous media.

## 2.2. Rheological and Mechanical Characterization of Zwitterionic Granular Hydrogels

Next, we evaluated rheological and mechanical properties of the generated granular hydrogels. First, rotational, and oscillatory measurements of microgels were conducted using a rheometer to characterize the effect of microgel size on rheological properties and injectability (Figure 3A). Viscosity measurements showed similar shear-thinning behavior of zwitterionic microgels for both sizes (Figure 3B). A linear relationship between viscosity and the shear rate in a log–log plot was observed, with decreasing viscosity with increasing shear rate, indicating viscous flow under shear stress and optimal injectability.

Oscillatory strain sweep tests were performed by repeated cycles of low (1%) and high (500%) strain. Under high shear stress, both microgel sizes changed from a solid ( $G' > G''$ ) to a liquid-like ( $G'' > G'$ ) state; once returned to a low shear mode, they showed excellent shear-recovery and self-healing properties, regardless of microgel size (Figure 3C). Similar shear-thinning and shear-recovery properties have been reported for microgels produced with mechanical fragmentation techniques.<sup>[7,34]</sup> Shear-thinning and self-healing hydrogels can be injected without

clogging of the needle, and they take the shape of the local environment and recover to their initial state after injection, making them ideal for homogenous encapsulation and delivery of cells to defects.<sup>[36]</sup> They are also cytoprotective during the injection process, protecting encapsulated cell membranes from shear-flow induced damage.<sup>[37]</sup>

Throughout the study, we have used microgels suspended at 6 wt%, matching the EWC of the bulk hydrogel. In this case, granular hydrogels will have no further swelling or shrinking after secondary crosslinking, making them suitable for cell encapsulation. However, we performed shear-thinning and shear-recovery tests on microgels suspended at lower (3%) and higher (9%) concentrations as well. As shown in Figure S6 of the Supporting Information, in both cases, the microgels have shear-thinning and shear-recovery properties, and the viscosity and modulus increase with the concentration. However, it should be noted that the 3% formulation has very low viscosity, making it unsuitable for injectable formulations, and the 9% formulation will have high levels of swelling, making it inadequate for cell encapsulation.

The yield stress required to induce flow and injectability, as determined by the crossover between the storage ( $G'$ ) and the loss ( $G''$ ) modulus, was also analyzed by performing a stress sweep test (Figure 3D). The yield stress was found to be  $195 \pm 23$  Pa and  $65 \pm 13$  Pa for 50 and 150  $\mu\text{m}$ -grid microgels, respectively (Figure 3D). The yield strain was also calculated by plotting ( $G'$ ) and ( $G''$ ) as a function of strain (Figure 3E) and determining the strain at crossover. The yield strain was higher for smaller 50  $\mu\text{m}$ -grid microgels compared to 150  $\mu\text{m}$ -grid microgels ( $19\% \pm 4\%$  vs  $5\% \pm 1\%$ ) (Figure 3E). Higher yield stress and strain for smaller microgels is due to the higher surface area of these microgels in a given volume. This leads to a higher degree of interparticle interactions, which in turn results in a larger force required for injection, and thus their ability to withstand more deformation before yielding.

For granular hydrogel characterizations, microgels were cast in PDMS molds of 6 mm in diameter and 2 mm in height and crosslinked with HRP and  $\text{H}_2\text{O}_2$  for 30 min resulting in granular hydrogel disks. We looked at granular hydrogel stability and swelling in PBS for 21 days. As shown in Figure 4A, granular hydrogels made of both sizes, were stable over 21 days of analysis with no signs of extensive swelling and degradation. This is due to the fact that microgels are already swollen up to their initial EWC before secondary crosslinking.

It should be noted that, as there is no significant swelling of the granular hydrogels after secondary crosslinking, the scaffold porosity also does not change over time. Granular hydrogels with tunable swelling and degradation properties, to control scaffold porosity over time, could be useful for different applications. However, since we use a minor fraction of GelMA as the crosslinker, the granular scaffold is prone to enzymatic degradation. We tested this by incubating granular hydrogels with collagenase ( $2 \text{ U mL}^{-1}$ ) over 21 days and measuring hydrogel swelling. As shown in Figure S7 of the Supporting Information, hydrogels with both microgel sizes swell more in presence of collagenase compared to PBS, which can be a sign of partial degradation of the GelMA. Moreover, the extent of swelling is more evi-

dent in the smaller microgels, probably due to the higher surface area further facilitating degradation. However, there was no major degradation happening even after 21 days, and the constructs are still fully stable.

Unconfined compression tests were done on both crosslinked and uncrosslinked granular hydrogels, to characterize the effect of secondary crosslinking on granular hydrogel stability and the effect of microgel size on mechanical properties (Figure 4B). We first compressed samples up to 15% at  $0.01 \text{ mm s}^{-1}$ , and the stress–strain curves of one loading–unloading cycle for both 50 and 150  $\mu\text{m}$ -grid microgels were plotted (Figure 4C). As evident in both curves, the energy dissipation, defined as the area between the loading and unloading curves, is higher for uncrosslinked microgels. This can be explained by the fact that the secondary crosslinking limits free motion of microgels, resulting in energy dissipation; the energy can be stored in the crosslinked network.

Compressive modulus was calculated as the slope of the linear region of the stress–strain curve (Figure 4D). The modulus of uncrosslinked microgels showed no significant size effect with  $1.1 \pm 0.3 \text{ kPa}$  for 50  $\mu\text{m}$  and  $0.9 \pm 0.3 \text{ kPa}$  for 150  $\mu\text{m}$ -grid microgels. However, the modulus was significantly increased for both microgel sizes after crosslinking and was higher for smaller microgels ( $6.2 \pm 0.1$  and  $4.0 \pm 0.3 \text{ kPa}$  for 50 and 150  $\mu\text{m}$ -grid microgels, respectively). This higher modulus for granular hydrogels made from smaller microgels is probably due to increased surface area and higher number of microgels per volume, which leads to increased crosslinking density as well as lower void space in these hydrogels.

Next, we compressed samples up to 80% of initial thickness, to ensure that we had granular hydrogels made of annealed and not just densely packed microgels, and also to see the point at which the construct yields. The crosslinked and uncrosslinked samples behaved very differently under high compression. Crosslinked microgels were able to withstand high levels of compressive load and return to their initial state after unloading (Movie S1), while the uncrosslinked microgels only spread and did not hold together (Movie S2). As shown before,<sup>[18a]</sup> the stress–strain curve of uncrosslinked microgels displays a very flat profile with no rupture point, because the pile of microgels cannot resist the force applied and immediately disperses under the testing probe. By contrast, annealed microgels can resist the force applied, similar to bulk materials, until the force causes the structure to rupture (Figure 4B). Similar trends were observed in our system comparing crosslinked and uncrosslinked microgels made of both sizes (Figure 4E).

The strain and stress at the failure point was measured for crosslinked granular hydrogels made of both sizes (Figure 4F). As expected because of the higher compressive modulus of granular hydrogels made of smaller microgels, these constructs were also more resilient and able to withstand more compressive force; and they can deform to a higher extent before being permanently ruptured. Zwitterionic granular hydrogels made of 50  $\mu\text{m}$ -grid microgels were able to withstand up to  $53.0\% \pm 1\%$  strain, compared to a  $37.4\% \pm 3\%$  strain for 150  $\mu\text{m}$ -grid microgels before rupturing, and they withstood up to six times more compressive stress (failure stress:  $12.0 \pm 1$  and  $2.8 \pm 0.3 \text{ kPa}$  for 50 and 150  $\mu\text{m}$ -grid microgels, respectively).

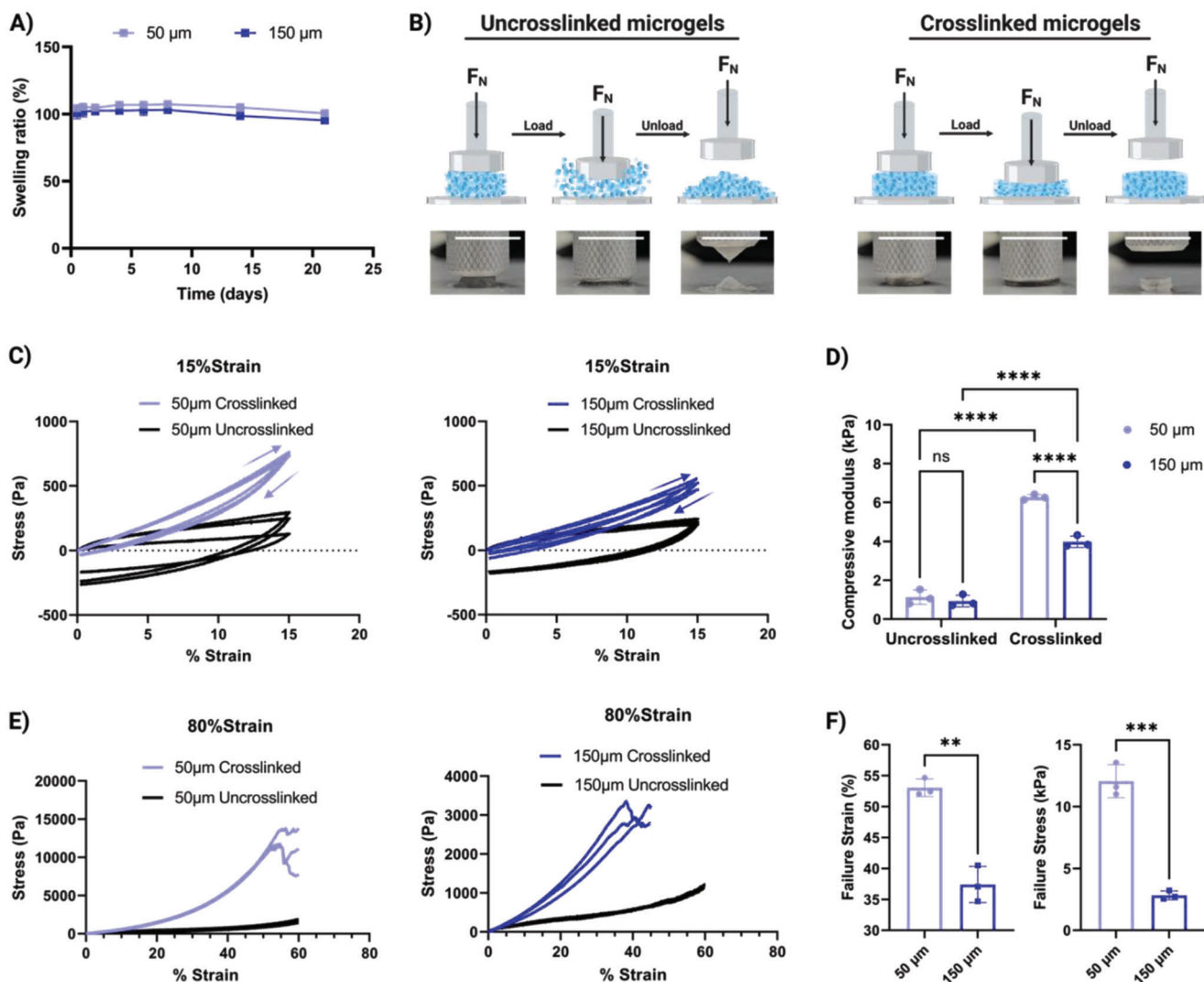


**Figure 4.** Mechanical properties of zwitterionic granular hydrogels. A) Swelling ratio of zwitterionic granular hydrogel in PBS. B) Schematic and reality photos of the compression testing of uncrosslinked and crosslinked microgels. Photographs show samples compressed up to 80% of their initial height. Scale bar: 1 cm. C) Stress–strain curve for granular hydrogels for one loading–unloading cycle of up to 15% strain. D) Compressive modulus calculated from linear region of stress–strain curve. E) Stress–strain curve for granular hydrogels up to 80% strain. F) Failure stress and strain measured at the rupture point for crosslinked microgels. Data are represented as mean  $\pm$  standard deviation. Statistical significance was determined using (D) a two-way ANOVA with a Tukey’s multiple comparisons test and (F) unpaired *t*-test ( $**p < 0.01$ ,  $***p < 0.001$ , and  $****p < 0.0001$ ) ( $n = 3$  replicates).

### 2.3. Zwitterionic Granular Hydrogels are Cytocompatible and Support Cell Proliferation and Migration

To investigate the potential of our zwitterionic granular hydrogels for cell encapsulation and cartilage tissue engineering, we encapsulated human primary chondrocytes collected from corrective surgeries of polydactyly patients in our hydrogels.<sup>[38]</sup> These chondrocytes, obtained from young patients, maintain higher proliferative and secretory properties compared to adult cells, and they have been reported to be nonimmunogenic and immunosuppressive, making them a promising cell source for allogeneic treatments.<sup>[39]</sup>

In our cell experiments, we investigated the effect of adding zwitterionic SBMA monomer into our CBAA granular hydrogels to study its effect on cell viability and ECM production

(Figure 1). It has been previously shown that while SBMA hydrogels are antifouling,<sup>[40]</sup> they support cell attachment more than other zwitterionic hydrogels.<sup>[21]</sup> This is probably due to the presence of anionic  $\text{SO}_3^-$  groups, which have been shown in a large body of research to improve cell attachment and result in augmented biological properties.<sup>[41]</sup> Moreover, incorporation of SBMA monomers into PEG hydrogels used for wound healing in vivo has been shown to improve different aspects of skin regeneration, as another indication of their superior bioactivity.<sup>[42]</sup> We therefore studied whether SBMA addition can improve encapsulated chondrocytes viability and chondrogenesis.

SBMA addition was performed by mixing the monomer with CBAA in the bulk hydrogel precursor solution to have a composite CBAA–SBMA (CB/SB) hydrogel. CB/SB granular hydrogels were made similar to pure CBAA (CB) hydrogels having 25 mol%



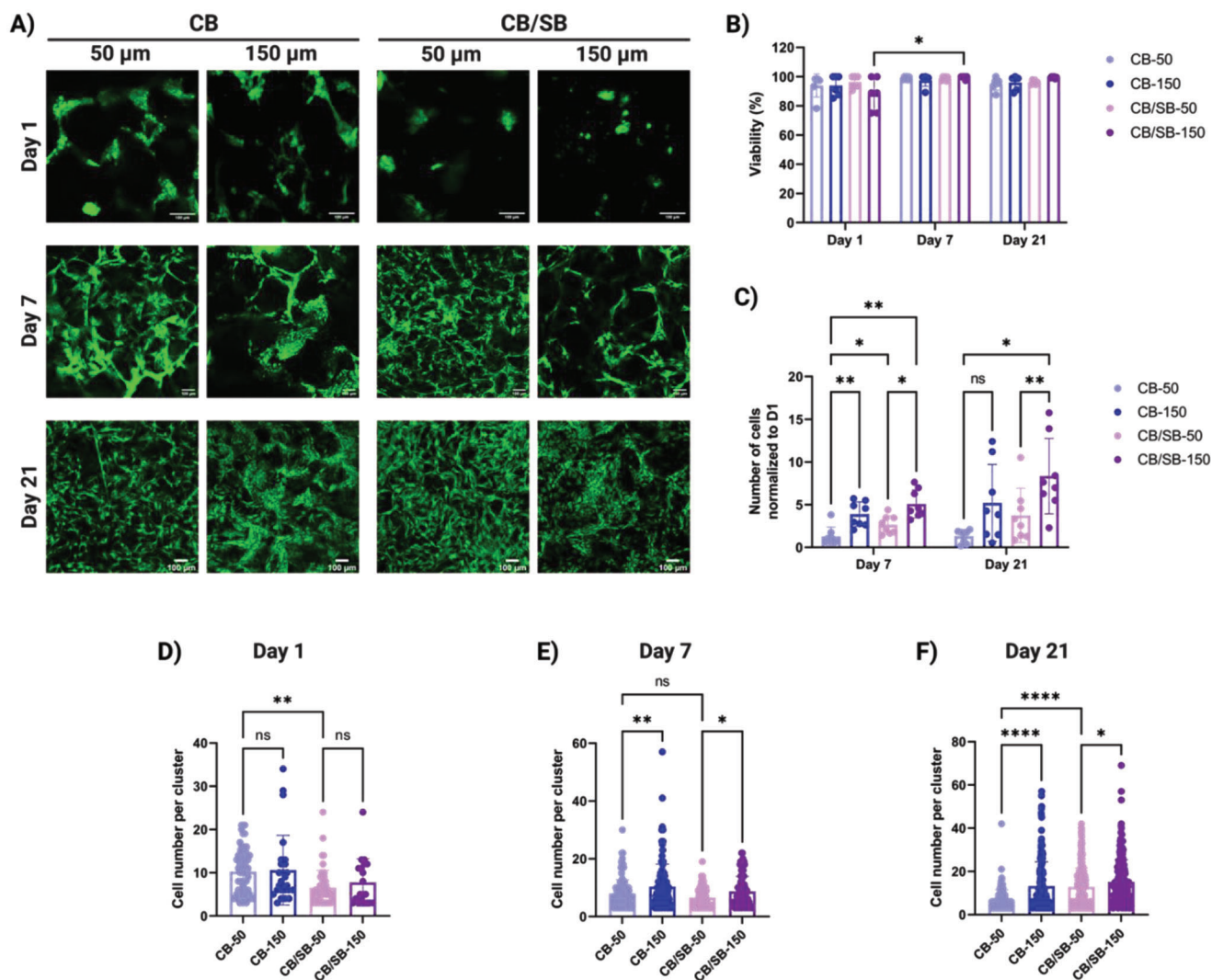


**Figure 5.** Cell encapsulation in zwitterionic granular hydrogels. A) Representative live–dead images. Scale bar 100  $\mu\text{m}$ . B) Calculated viability ( $n = 3$  hydrogels, 3 images per hydrogel). C) Number of counted cells at day 7 and 21 normalized to number of cells at day 1 ( $n = 3$  hydrogels, 3 images per hydrogel). D–F) Number of cells calculated per cluster after 1, 7, and 21 days of culture. Data are represented as mean  $\pm$  standard deviation. Statistical significance was determined using (B,C) a two-way or (D–F) one-way ANOVA with a Tukey’s multiple comparisons test (nonsignificant (ns)  $p > 0.05$ ,  $*p < 0.05$ ,  $**p < 0.01$ ,  $***p < 0.001$ , and  $****p < 0.0001$ ).

SBMA in the bulk hydrogel formulation. Qualitative and quantitative Fourier-transform infrared spectroscopy (FTIR) of microgels, together with appropriate calibration standards, allowed us to determine the amount of SBMA in the microgels, which was close to the theoretical amount loaded (Figure S8, Supporting Information). We compared microgel diameter for CB and CB/SB microgels made with two grids and observed no significant difference in average microgel diameter or in its distribution for each microgel size made with different monomer compositions (Figure S9A, Supporting Information). We also observed no difference in average void fraction, pore size, and compressive modulus of CB versus CB/SB granular hydrogels, confirming that the two monomer compositions do not affect granular hydrogel properties (Figure S9B–D, Supporting Information).

We investigated chondrocyte encapsulation in our CB and CB/SB zwitterionic granular hydrogels, each made with two dif-

ferent grid sizes (50 and 150  $\mu\text{m}$ ) to study the effect of monomer type and microgel size on cell response. The four investigated groups are named as CB-50, CB-150, and CB/SB-50 and CB/SB-150 based on monomer composition and grid size. Human chondrocytes were mixed with microgels and cast in cylindrical PDMS molds, 6 mm in diameter and 2 mm in height, and were then enzymatically crosslinked for 30 min at 37  $^{\circ}\text{C}$  by addition of HRP and  $\text{H}_2\text{O}_2$ . This resulted in a microporous hydrogel with chondrocytes encapsulated in the micrometer-sized pores between microgels. Chondrocytes were encapsulated at 10 million cells  $\text{mL}^{-1}$  and cultured for 3 weeks in chondrogenic media. Representative live–dead images of cells encapsulated in different hydrogels and at different timepoints are shown in Figure 5A. For all hydrogels and timepoints, high cell viability of over 90% was observed (Figure 5B), indicating no cytotoxicity derived from the prepared materials.

As evident in Figure 5A, encapsulated cells were able to proliferate and migrate inside the granular hydrogels, as the cell area increases over time in all hydrogels, and the pores initially devoid of cells become filled with cells. To semiquantitatively analyze cell proliferation, we counted the number of cell nuclei stained with Hoechst at each timepoint and normalized it to the number of nuclei on the first day. As expected, the calculated number was bigger than 1 in all hydrogels and at all timepoints, and it was increasing for each hydrogel at day 21 compared to day 7, indicating continuous proliferation over 21 days of culture (day 7:  $1.2 \pm 1$ ,  $3.8 \pm 1$ ,  $2.6 \pm 1$ , and  $5.0 \pm 1$ , day 21:  $1.3 \pm 1$ ,  $5.2 \pm 4$ ,  $3.7 \pm 3$ , and  $8.3 \pm 4$  for CB-50, CB-150, CB/SB-50, and CB/SB-150 hydrogels, respectively) (Figure 5C). It is noteworthy that for both hydrogel types and at both timepoints, proliferation was higher for hydrogels made of 150  $\mu\text{m}$ -grid microgels compared to 50  $\mu\text{m}$ -grid microgels, indicating that the greater porosity and pore size of these hydrogels leads to increased proliferation rate. Also, when comparing different hydrogel types having the same microgel sizes, we observe that, especially at day 7, the proliferation rate is higher in CB/SB hydrogels compared to CBAA hydrogels, indicating the positive effect of SBMA addition.

Another morphological characteristic of encapsulated cells is that they can spread through the pores, making an interconnected cellular network, and they aggregate and form clusters in the pores (Figure 5A). We quantified the number of cells per cluster in each hydrogel and at each timepoint, as indicated in the Experimental Section, using ImageJ (Figure 5D–F). At day 1, there was no significant difference in the number of cells per cluster for different microgel sizes, but there were more cells per clusters in CBAA hydrogels compared to CB/SB hydrogels ( $10.1 \pm 5$ ,  $10.6 \pm 8$ ,  $6.5 \pm 4$ , and  $7.7 \pm 5$  for CB-50, CB-150, CB/SB-50, and CB/SB-150 hydrogels, respectively), probably due to the higher antifouling properties of CBAA hydrogels pushing cells toward aggregation (Figure 5D). However, at day 7 this was not the case, and while there was no difference between CB and CB/SB hydrogels, the number of cells per cluster was higher for hydrogels with bigger microgel size and larger porosities ( $8.0 \pm 5$ ,  $10.3 \pm 7$ ,  $6.5 \pm 3$ , and  $8.7 \pm 5$  for CB-50, CB-150, CB/SB-50, and CB/SB-150 hydrogels, respectively), which indicates that the effect of porosity is stronger than that of material at later timepoints (Figure 5E). The trend of higher numbers of cells per cluster for hydrogels with larger porosity was the same at day 21, but there were also more cells per cluster in CB/SB hydrogels compared to CBAA hydrogels, especially for 50  $\mu\text{m}$ -grid microgels ( $6.9 \pm 4$ ,  $13.2 \pm 11$ ,  $12.9 \pm 8$ , and  $15.2 \pm 10$  for CB-50, CB-150, CB/SB-50, and CB/SB-150 hydrogels, respectively), probably due to the higher proliferation rate in these hydrogels having the same porosity (Figure 5F).

It is also interesting that when comparing the number of cells per cluster for each hydrogel over time, there is no significant difference for CB hydrogels; however, the number slightly increases for CB/SB hydrogels from day 7 to day 21, probably due to the higher proliferation rate in these hydrogels. As it was shown that cells were proliferating and increasing in number over time, the fact that the cluster size is not increasing significantly, shows that proliferated cell are able to move and migrate within the construct. These data confirm that all of our zwitterionic granular hydrogels support proliferation and migration of encapsulated primary chondrocytes throughout the constructs over 21 days of culture.

Another characteristic of the hydrogels that affects chondrocytes' behavior is the scaffold stiffness. Different results have been reported for how stiffness of the scaffold affects chondrocyte metabolism, with soft hydrogels within the range of  $\approx 1$ – $10$  kPa shown to be favorable for cells.<sup>[43]</sup> However, it should be noted that since cells in granular hydrogels are encapsulated in the pores between microgels, the effect of the stiffness of the granular hydrogel or of individual microgels on cell behavior will be different from that of a bulk hydrogel. What is interesting with the current system is that microgels with different sizes that result in granular hydrogels with different porosities are made with the same swollen hydrogel, and they therefore have the same stiffness. This also holds true for microgels made of CBAA or CBAA–SBMA, as both bulk hydrogels have a similar modulus (Figure S5C, Supporting Information). Thus, this system can be a good example of decoupling the effect of microgel stiffness from granular hydrogel porosity. However, a more detailed analysis of surface properties and stiffnesses of microgels at a microlevel needs to be done to further elaborate on this subject.

#### 2.4. Enhanced Chondrogenesis with Increased Porosity and Incorporation of SBMA in Zwitterionic Granular Hydrogels

Cell-laden injectable hydrogels delivered to cartilage defects are expected to provide an optimal environment for cells to produce ECM over time and eventually, ideally, replace the whole scaffold with healthy new tissue. To replicate the intended function of the tissue, the produced ECM should be similar to the native tissue in composition and homogenous throughout the construct. It has previously been shown that cartilage ECM deposition in granular hydrogels is more homogenous, in the areas between microgels, compared to bulk hydrogels both *in vitro* and *in vivo*, where the produced ECM is mostly pericellular.<sup>[7]</sup>

We studied the ECM produced by encapsulated human chondrocytes in our zwitterionic granular hydrogels. Human chondrocytes were encapsulated in granular hydrogels and cultured in chondrogenic media containing transforming growth factor- $\beta 3$  (TGF- $\beta 3$ ) as  $10$  ng mL<sup>-1</sup> for 21 days. At the end of the 21 days, samples were fixed and prepared for histological analysis and stained for glycosaminoglycans (GAGs) and collagen type II as major components of articular cartilage, as well as for collagen type I. Representative images of stained samples as well as native human articular cartilage controls are shown in Figure 6A, where GAGs are stained red in safranin O staining, and collagens are stained brown in immunohistochemistry. As seen in Figure 6A homogeneous deposition of GAGs, collagen type II, and collagen type I were observed in the void spaces between the microgels for all granular hydrogels.

The extent of tissue maturation in samples was analyzed with compressive modulus measurements at day 21 (Figure 6B). An increase in compressive modulus was observed for all samples from  $\approx 4$ – $6$  kPa at day 1 to  $\approx 20$ – $50$  kPa at day 21, due to ECM secretion (compressive modulus at day 21:  $16.9 \pm 6$ ,  $27.2 \pm 8$ ,  $39.7 \pm 15$ , and  $38.8 \pm 10$  kPa for CB-50, CB-150, CB/SB-50, and CB/SB-150 hydrogels, respectively). There was more tissue maturation for samples with 150  $\mu\text{m}$ -grid microgels in both materials, as evidenced by an increase in compressive modulus compared to day 1. This was probably due to the larger porosity and greater

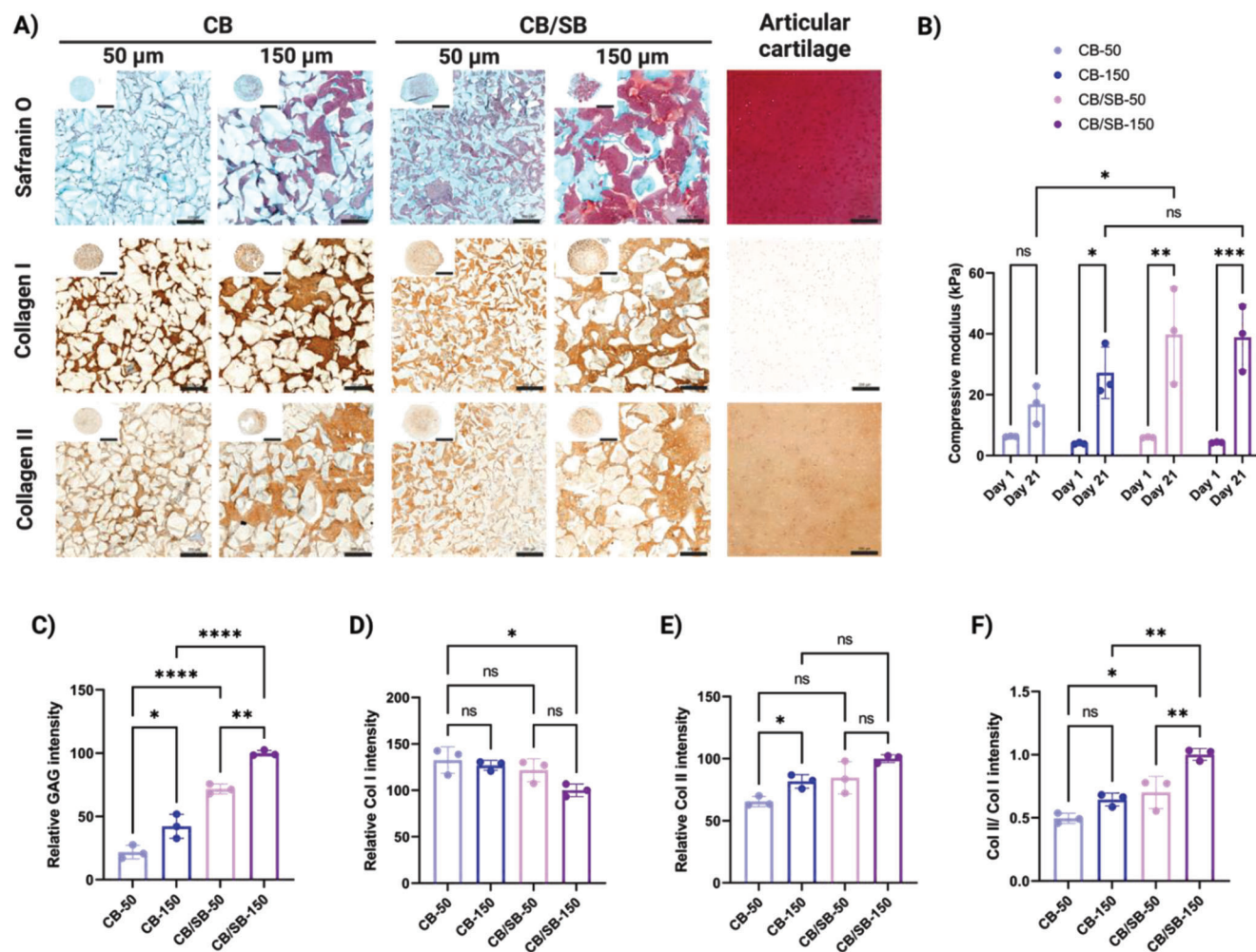


**Figure 6.** In vitro chondrogenesis of human chondrocytes encapsulated in zwitterionic granular hydrogels. A) Representative histological and immunohistological staining for GAG, collagen I and collagen II after 21 days of in vitro culture. Scale bar: 200  $\mu\text{m}$  and 1 mm in zoom out inserts. B) Compression modulus of the constructs after 3 weeks of culture. C–E) Semiquantitative evaluation of deposited GAG, collagen I and collagen II intensity, respectively, relative to native human articular cartilage. F) Ratio of collagen II to collagen I intensity. Data are represented as mean  $\pm$  standard deviation. Statistical significance was determined using a two-way (B) or one-way (C–F) ANOVA with a Tukey's multiple comparisons test (nonsignificant (ns)  $p > 0.05$ ,  $*p < 0.05$ ,  $**p < 0.01$ ,  $***p < 0.001$ , and  $****p < 0.0001$ ) ( $n = 3$  replicates).

cell proliferation in these samples, as shown in the previous section. Also, there was slightly more maturation in CB/SB granular hydrogels compared to CBAA, again due to greater cell proliferation and probably the higher metabolic activity of cells in these hydrogels. It should be noted that the compressive modulus of the samples at this point is low compared to native cartilage ( $\approx 1$ – $1.5$  MPa). However, as we observed a  $\approx 10$ -fold increase in the compressive modulus of scaffolds over only 3 weeks of in vitro culture, we predict that additional material optimization and even longer culture times will lead to further increase and therefore extended tissue maturation and higher compressive modulus.

Semiquantitative analyses were performed by comparing GAGs, collagen type II, and collagen type I intensities to native human articular cartilage controls as shown in Figure 6A and normalizing to the sample with the highest intensity (CB/SB-150). A higher GAG and collagen type II and lower collagen type I secretion is characteristic of optimal chondrogenesis. As shown in Figure 6C, relative GAGs intensity was significantly

higher for granular hydrogels with higher porosity (150  $\mu\text{m}$  vs 50  $\mu\text{m}$ -grid microgels) and for those made of CB/SB compared to CBAA (GAG intensity:  $21.7 \pm 5$ ,  $42.2 \pm 9$ ,  $71.7 \pm 4$ , and  $100.0 \pm 2$  for CB-50, CB-150, CB/SB-50, and CB/SB-150 hydrogels, respectively). In all the samples there was extensive collagen type I secretion, which is normally secreted in in vitro chondrogenesis studies.<sup>[44]</sup> There was no difference in collagen I intensity of CBAA hydrogels with different porosities, but the intensity was lower for CB/SB hydrogels with larger microgels, demonstrating enhanced chondrogenesis (Figure 6D) (collagen I intensity:  $132.6 \pm 14$ ,  $126.9 \pm 5$ ,  $121.5 \pm 12$ , and  $100.0 \pm 6$  for CB-50, CB-150, CB/SB-50, and CB/SB-150, respectively). Similar trends in GAG intensity were observed for collagen II intensity (Figure 6E) and Col II/Col I ratio (Figure 6F) (collagen II intensity:  $65.4 \pm 4$ ,  $81.7 \pm 5$ ,  $84.6 \pm 13$ , and  $100.0 \pm 3$  for CB-50, CB-150, CB/SB-50, and CB/SB-150 hydrogels, respectively), showing overall improved chondrogenesis with increased porosity and incorporation of SBMA. Here we report for the first time that a purely

zwitterionic hydrogel supports chondrogenesis of encapsulated cells allowing for cell proliferation and ECM deposition. However, the quality and extent of ECM secretion could be enhanced to achieve more collagen type II and less collagen type I secretion.

### 3. Conclusion

This study presents a simple and yet versatile strategy to produce zwitterionic granular hydrogels, which can be used as an injectable formulation for repairing cartilage defects by delivering cells in a biocompatible and nonimmunogenic scaffold. The secondary enzymatic crosslinking used in this system allows for in situ annealing in a mild and cytocompatible manner, providing long-term stability and support for cells. The hydrogel showed optimal shear-thinning and shear-recovery properties and after secondary enzymatic crosslinking, resulted in a microporous scaffold with 13–20% porosity, depending on microgel size. We observed that proliferation and chondrogenesis of encapsulated cell are enhanced in granular hydrogels with larger porosity (150  $\mu\text{m}$ -grid microgels vs 50  $\mu\text{m}$ -grid) and when the SBMA monomer is incorporated into the CBAA granular hydrogels. Overall, this versatile and highly biocompatible platform strategy shows great promise in using different zwitterionic monomers for multiple tissue engineering applications. Future work will include development of optimally degradable microgels to further support tissue maturation. This can be done with incorporation of hydrolysable or matrix metalloproteinase-cleavable linkers in the system and tuning the degradation rate to match that of new ECM formation. In vivo studies are needed to further evaluate in vivo compatibility and efficacy of the system. This can be done by injection of cells and zwitterionic microgels to fill and regenerate chondral defects compared to cells injected alone or with other carriers.

### 4. Experimental Section

**Materials:** Gelatin from porcine skin Type A, methacrylic anhydride, tyramine hydrochloride, acryloyl chloride, fluorescein *o*-acrylate, *N,N*-diisopropylethylamine (DIPEA), (2 (methacryloyloxy)ethyl)dimethyl-(3-sulfopropyl)ammonium hydroxide (SBMA), LAP, sodium pyruvate, HRP,  $\text{H}_2\text{O}_2$ , anhydrous tetrahydrofuran (THF), and collagenase from *Clostridium histolyticum* were purchased from Sigma. Beta-propiolactone and *N,N*-dimethylformamide (DMF) were purchased from Acros. *N*-(3-(Dimethylamino)propyl)acrylamide (DMAPA) and L-Ascorbic acid 2 phosphate sesquimagnesium salt hydrate were purchased from TCI chemicals. Gentamycin, Dulbecco's modified eagle medium (DMEM 31966) and fetal bovine serum (FBS) were obtained from Gibco. ITS+ Premix Universal Culture Supplement was bought from Corning and fibroblast growth factor-2 (FGF-2) and transforming growth factor- $\beta$ 3 (TGF- $\beta$ 3) from PreproTech. All other solvents and reagents were purchased from Sigma.

**CBAA Synthesis:** The monomer was synthesized according to a literature procedure,<sup>[45]</sup> with minor modifications. In a 100 mL one-neck round-bottom flask equipped with a magnetic stirring bar, DMAPA (8.9 g, 57.28 mmol, 1 eq) was dissolved in 60 mL anhydrous THF and the flask was sealed with dropping funnel and placed to  $-10^\circ\text{C}$  ethanol bath. Beta-propiolactone (5 mL, 79.86 mmol, 1.4 eq) dissolved in 15 mL anhydrous THF was added to the dropping funnel and slowly dropped into the above solution under stirring for  $\approx 2$  h. Afterward, the reaction mixture was allowed to warm to room temperature and stirred overnight. Then the resulting white suspension was placed to the freezer for another 24 h at  $-20^\circ\text{C}$  to precipitate the product. Then the mixture was filtered through sin-

tered glass funnel (S4 porosity) washed with dry diethyl ether and the product was obtained with vacuum filter, washed several times with cold ether, and dried overnight under high vacuum.  $^1\text{H}$  NMR (Bruker Ultra shield 400 MHz) in  $\text{D}_2\text{O}$  revealed successful and pure synthesis of the product. The chemical synthesis scheme can be found in Figure S1 of the Supporting Information, and  $^1\text{H}$  NMR spectroscopy can be found in Figure S2 of the Supporting Information.

**TyrAA Synthesis:** The monomer was synthesized according to a literature procedure,<sup>[46]</sup> with some modifications. In a 100 mL round-bottom flask equipped with a magnetic stirring bar, tyramine hydrochloride (2.0 g, 11.52 mmol, 1 eq) was dissolved in 32 mL DMF. DIPEA (6 mL, 34.55 mmol, 3 eq) was added; the solution was degassed by bubbling with nitrogen for 15 min and cooled in  $0^\circ\text{C}$  ice bath. Acryloyl chloride (1.2 mL, 14.97 mmol, 1.3 eq) dissolved in 3 mL DMF was slowly dropped into the above solution under vigorously stirring. The reaction mixture was allowed to warm to room temperature and stirred overnight. The solvent was removed on a rotary evaporator and redissolved in  $\approx 10$  mL ethyl acetate and then transferred to  $-20^\circ\text{C}$  to allow for crystallization of the product overnight. The product was obtained with vacuum filter, washed with cold chloroform, and dried overnight under vacuum.  $^1\text{H}$  NMR (Bruker Ultra shield 400 MHz) in  $\text{D}_2\text{O}$  revealed successful and pure synthesis of the product. The chemical synthesis scheme can be found in Figure S1 of the Supporting Information, and  $^1\text{H}$  NMR spectroscopy can be found in Figure S3 of the Supporting Information.

**GelMA Synthesis:** GelMA was synthesized as previously described,<sup>[33]</sup> with some modifications. In a round bottom flask, gelatin type A was dissolved in 0.1 M carbonate-bicarbonate buffer at pH 9 as 10 wt% solution and warmed up to  $50^\circ\text{C}$  under vigorous stirring. Methacrylic anhydride was added to the solution in five steps every 30 min, and after every addition, pH was adjusted with NaOH to 9. After the last addition, the reaction was diluted twofold and left to react for another 60 min. At the end, pH was adjusted to 7.4 and the product was cleaned by subsequent dialysis against ultrapure water at  $40^\circ\text{C}$  for 4 days. The solution was filtered, lyophilized, and stored at  $-20^\circ\text{C}$  until use. The DS was estimated with  $^1\text{H}$  NMR (Bruker Ultra shield 400 MHz) in  $\text{D}_2\text{O}$ . GelMA lysine integration signal (2.95–3.05 ppm) was compared to unmodified gelatin lysine integration signal (2.95–3.05 ppm). Phenylalanine signal (7.2–7.5 ppm) was used as an internal reference. DS was found to be  $\approx 73\%$ .

**Zwitterionic Bulk Hydrogel Preparation:** Bulk zwitterionic hydrogels were produced by photopolymerization of zwitterionic monomers and TyrAA using GelMA as the crosslinker and LAP as photoinitiator. The solution was prepared by dissolving zwitterionic monomers at 2.5 M and GelMA as 0.004 M (0.16 mol%) final concentration in Milli-Q water in a  $37^\circ\text{C}$  water bath. TyrAA was first dissolved as 50 wt% in DMF and then added to the solution, to have a final concentration of 0.125 M (5 mol%/mol%). The solution was degassed with nitrogen for 10 min; then LAP was added to have a final concentration of 0.05%. The solution was then injected between two glass slides with a 1 mm polytetrafluoroethylene spacer. Photopolymerization was initiated by UV-vis (405 nm, 30 min), and the resulting hydrogels were dialyzed in deionized water for at least 5 days. At the end of dialysis, 4 mm hydrogel disks were punched, weighted, and then freeze dried to measure EWC of the hydrogels. EWC was measured as the ratio of water mass (swollen hydrogel weight minus dried hydrogel weight) to swollen hydrogel mass. For CBAA hydrogel preparation, 2.5 M CBAA monomer was used, whereas for CBAA-SBMA hydrogels 75:25 mol ratio of the two monomers was used (1.875 M CBAA and 0.625 M SBMA). To prepare fluorescently labeled hydrogels, fluorescein *o*-acrylate comonomer was added to the starting monomer solution at a final concentration of 0.018 wt%.

**Zwitterionic Granular Hydrogel Preparation:** Zwitterionic microgels were made by mechanical fragmentation. Equilibrated bulk zwitterionic hydrogels were cut into small pieces and transferred into a 10 mL custom-made extruder connected to a metal sieve with mesh width of 150 and 50  $\mu\text{m}$ . For 150  $\mu\text{m}$  grid microgels, bulk gels were manually sieved three consecutive times with the 150  $\mu\text{m}$  mesh, and for 50  $\mu\text{m}$ -grid microgels, the resulting microgels were additionally sieved another three times with the 50  $\mu\text{m}$  mesh. Microgels were then sterilized by precipitation in ethanol, dried overnight in vacuum oven, resuspended in sterile water, and

lyophilized. To make zwitterionic granular hydrogels, the lyophilized microgels were first resuspended as 6 wt% in PBS buffer. To prepare 100  $\mu\text{L}$  of granular hydrogel, 90  $\mu\text{L}$  of microgels was mixed with 5  $\mu\text{L}$  of HRP (2 mg  $\text{mL}^{-1}$ , 300 U  $\text{mL}^{-1}$ ) and 5  $\mu\text{L}$  of  $\text{H}_2\text{O}_2$  (0.1%) in cylindrical PDMS molds with 6 mm in diameter and 2 mm in height and incubated for 30 min.

**Swelling and EWC Measurement:** For swelling of the bulk hydrogels, 6 mm hydrogel disks were punched after photocrosslinking, weighed, and transferred to 1.5 mL Eppendorf tubes containing 1 mL 1 $\times$  PBS, and incubated at 37  $^\circ\text{C}$ . At regular intervals, supernatants were removed, and the samples were weighed. The swelling ratio was determined as the ratio of hydrogel mass at a given time point divided by its initial mass and reported as a percentage. For EWC measurement of the bulk hydrogels, the swollen hydrogels after 5 days (no further swelling was observed after this point) were freeze dried. EWC was calculated as the ratio of water mass (swollen hydrogel weight minus dried hydrogel weight) to the swollen hydrogel mass. For swelling of granular hydrogels, hydrogel disks were made as previously described using 6 mm PDMS disks, then transferred to 1.5 mL Eppendorf tubes containing either 1 mL PBS 1 $\times$  or collagenase as 2 U  $\text{mL}^{-1}$  in PBS and incubated at 37  $^\circ\text{C}$ . Measurements and calculations were done similar to with bulk hydrogels. Collagenase solution was refreshed every other day to ensure continuous enzyme activity.

**Microgel Size Distribution:** Bulk zwitterionic hydrogels were made as previously described with 0.018% fluorescein *o*-acrylate in the hydrogel precursor solution. The fluorescently labeled zwitterionic microgels were then prepared using the mechanical fragmentation method described before. Lyophilized microgels were then resuspended in PBS at a low concentration of  $\approx 0.5\%$ , to permit microgel separation under the microscope. Microgel size was determined by dispersing the microgels into glass slides and imaging with a fluorescent microscope (SP8, Leica). Microgel diameter was evaluated using ImageJ software with the particle analysis tool.

**Granular Hydrogel Porosity Measurement:** The fluorescently labeled zwitterionic microgels were prepared and crosslinked as previously described to obtain fluorescent granular hydrogels. Samples were imaged by confocal microscopy (SP8, Leica). Void fraction and pore size were determined by converting the stacks into single images and using a threshold to select the void spaces. Cross-sectional areas occupied by void spaces were determined for each image and averaged for the whole stack.

**Rheological Characterization:** Rheological analysis was carried out on an Anton Paar MCR 301 rheometer equipped with 10 mm parallel plate geometry (PP10, Anton Paar) and a peltier element with thermal hood (HPTD 200, Anton Paar). All tests were performed at 25  $^\circ\text{C}$ . Humidity in the thermal hood was controlled by placing a wet tissue inside the chamber to prevent drying of the sample. Ramped shear rate (0.01–300  $\text{s}^{-1}$ ) and shear stress sweeps (1 Hz, 1–1000 Pa, ramp logarithmic) were performed to evaluate the shear-thinning behavior and yield point, respectively. To evaluate the shear-recovery properties, microgels were repeatedly exposed to cycles of alternating low (1 Hz, 1% strain) and high strain (1 Hz, 500% strain). All rheological characterizations were performed on 6 wt% microgel. Each test was repeated three times with a new sample. In all experiments, the gap size was adjusted to 600  $\mu\text{m}$  for 50  $\mu\text{m}$  microgels and to 1600  $\mu\text{m}$  for 150  $\mu\text{m}$  microgels.

**Compression Testing:** Unconfined compression experiments were performed on a TA.XTplus texture Analyzer (Anton Paar) equipped with a 500 g load cell. For each sample (6 mm in diameter and 2 mm in height), a preload was applied to the sample until it reached full contact with the plate and was then allowed to relax completely. Samples were compressed at a rate of 0.01  $\text{mm s}^{-1}$  until they reached 15% or 80% strain. The compressive modulus was extracted from the slope of the first linear part of the stress versus strain curve.

**Primary Human Chondrocyte Isolation and Culture:** Primary human chondrocytes were collected from corrective surgeries of polydactyly patients after informed consent from legal guardians (Kantonale Ethikkommission Zurich, license number PB\_2017-00510), as described previously.<sup>[38]</sup> Cartilage pieces were finely sliced ( $\approx 0.5$  mm thickness), washed extensively in PBS with 50  $\mu\text{g mL}^{-1}$  gentamicin (Gibco), and digested in collagenase solution (DMEM (Gibco), 1000 CDU  $\text{mL}^{-1}$  colla-

nase from Clostridium histolyticum, 2 V% FBS (Gibco), and 1 $\times$  antibiotic–antimycotic (Anti–Anti, Gibco) overnight with gentle shaking at 37  $^\circ\text{C}$ . The resulting cell suspension was passed through a 40  $\mu\text{m}$  cell strainer before collecting the cell pellet by centrifugation (500 rcf, 10 min). The cells were plated at  $\approx 10\,000$  cells  $\text{cm}^{-2}$  and expanded in DMEM, 10 V% FBS, 1 $\times$  Anti–Anti, and 10 ng  $\text{mL}^{-1}$  FGF-2 at 37  $^\circ\text{C}$ , 5%  $\text{CO}_2$ , and 95% humidity. After the first passage, the seeding density was reduced to  $\approx 3000$  cells  $\text{cm}^{-2}$  and Anti–Anti was exchanged for 10  $\mu\text{g mL}^{-1}$  gentamicin.

**Cell Encapsulation in Zwitterionic Granular Hydrogels and In Vitro Chondrogenesis:** Cells at passage 2 were trypsinized and mixed with zwitterionic microgels (6 wt%) at a final density of 10 million cells  $\text{mL}^{-1}$ . The microgel–cell suspension was then gently mixed with crosslinkers and crosslinked as described previously, in cylindrical PDMS molds with 6 mm diameter and 2 mm height. Scaffolds were cultured in chondrogenic medium containing DMEM, 10  $\mu\text{g mL}^{-1}$  gentamicin, 1% ITS+, 50  $\mu\text{g mL}^{-1}$  L-ascorbate-2-phosphate, 40  $\mu\text{g mL}^{-1}$  L-proline, and 10 ng  $\text{mL}^{-1}$  TGF- $\beta$ 3. Medium was changed every second day. In vitro experiments were stopped after 21 days for viability, mechanical and histological analysis.

**Cell Viability:** To assess viability, samples were stained with a medium supplemented with 1  $\mu\text{m}$  CalceinAM, 1  $\mu\text{m}$  propidium iodide (PI) and 0.3  $\mu\text{m}$  Hoechst for 1 h. Imaging was performed on a Leica SP8 microscope equipped with a 10 $\times$  and 20 $\times$  objective. 100  $\mu\text{m}$  Z-stacks were acquired with 5  $\mu\text{m}$  steps. Viability was assessed by counting viable (CalceinAM+) and dead (PI+) cells throughout the entire range and dividing the number of viable cells by the total number of viable cells plus dead cells. Proliferation was calculated as the ratio of the number of cell nuclei (Hoechst+) at each timepoint divided by the number of cell nuclei at day 1. Cell clustering evaluation after 1, 7, and 21 days was manually performed with the ImageJ software, using cluster identifier plugin with identifying cell nuclei clusters as cell populations with more than three cells in proximity.

**Histology and Immunohistochemistry:** Samples were fixed in 4% paraformaldehyde for 4 h, dehydrated in an ethanol sequence, embedded in paraffin wax (Milestone Logos) and cut into 5  $\mu\text{m}$  sections on a microtome. Samples were progressively deparaffinized and rehydrated before staining. Brightfield images of stained sections were recorded on a 3DHi-tech Panoramic 250-slide scanner and visualized with the case viewer 2.4 software. Safranin O staining: sections were first stained in Weigert's Iron Hematoxylin solution for 5 min, washed in deionized water and differentiated in 1% acid–alcohol for 2 s. Sections were again washed and stained in 0.02% Fast Green solution for 1 min and rinsed with 1% acetic acid for 30 s. Finally, sections were stained in 1% Safranin O for 30 min, dehydrated to xylene and mounted. Collagen I and II immunohistochemistry: antigen retrieval was first performed in hyaluronidase (1200 U  $\text{mL}^{-1}$ ) at 37  $^\circ\text{C}$  for 30 min. Sections were blocked with 5% BSA in PBS for 1 h. Primary antibody, rabbit anticollagen I (1:1500, ab138492, Abcam) and mouse anticollagen II (1:20, II-II6B3-s, DSHB Hybridoma) were dissolved in 1% BSA in PBS, and sections were incubated overnight at 4  $^\circ\text{C}$ . Sections were then incubated with the secondary antibody, goat anti-rabbit IgG-HRP for rabbit anti-collagen I (1:1000, ab6721, Abcam) or goat anti-mouse IgG-HRP for collagen II (1:1000, ab6789, Abcam) in 1% BSA in PBS for 1 h and developed with the DAB substrate kit (ab64238, Abcam) for 5 min. Sections were stained with Weigert's iron hematoxylin (Thermo Fisher Scientific) for 3 min, destained in 1% acid–alcohol, blued in 0.1%  $\text{Na}_2\text{CO}_3$ , dehydrated to xylene, and mounted.

**Statistical Analyses:** All data are presented with individual data points on the graphs, bar plots with errors bars representing mean  $\pm$  standard deviation with  $n \geq 3$ . Statistical analyses were performed in GraphPad Prism 9.2.0 software. A one-way or two-way ANOVA with Tukey's multicomparison test was used to analyze the data. A level of  $p < 0.05$  was considered significant. The  $p$ -values for statistical significance are represented with stars ( $*p < 0.05$ ,  $**p < 0.01$ ,  $***p < 0.001$ , and  $****p < 0.0001$ ).

## Supporting Information

Supporting Information is available from the Wiley Online Library or from the author.

## Acknowledgements

The authors would like to thank the Swiss National Science Foundation for providing financial support (Grant No. 315230-192656 to M.Z.-W.). Thanks also to the ScopeM center at ETH for providing technical support and David Fercher for primary human chondrocyte isolation. Illustrations and figures were created with BioRender.com

Open access funding provided by Eidgenössische Technische Hochschule Zurich.

## Conflict of Interest

The authors declare no conflict of interest.

## Data Availability Statement

The data that support the findings of this study are openly available in [ETH Repository] at [<http://hdl.handle.net/20.500.11850/607782>], reference number [607782].

## Keywords

carboxybetaine acrylamide, cartilages, granulars, hydrogels, injectable hydrogels, microgels, zwitterionic hydrogels

Received: July 17, 2023

Revised: July 24, 2023

Published online:

- [1] a) Y. P. Singh, J. C. Moses, N. Bhardwaj, B. B. Mandal, *J. Mater. Chem. B* **2018**, *6*, 5499; b) P. Zarrintaj, M. Khodadadi Yazdi, M. Youssefi Azarfam, M. Zare, J. D. Ramsey, F. Seidi, M. Reza Saeb, S. Ramakrishna, M. Mozafari, *Tissue Eng., Part A* **2021**, *27*, 821.
- [2] a) X. Lin, C. T. Tsao, M. Kyomoto, M. Zhang, *Adv. Healthcare Mater.* **2022**, *11*, 2101479; b) M. Liu, X. Zeng, C. Ma, H. Yi, Z. Ali, X. Mou, S. Li, Y. Deng, N. He, *Bone Res.* **2017**, *5*, 17014; c) J. Xu, Q. Feng, S. Lin, W. Yuan, R. Li, J. Li, K. Wei, X. Chen, K. Zhang, Y. Yang, *Biomaterials* **2019**, *210*, 51.
- [3] a) A. Armiento, M. Stoddart, M. Alini, D. Eglin, *Acta Biomater.* **2018**, *65*, 1; b) J. Wu, Q. Chen, C. Deng, B. Xu, Z. Zhang, Y. Yang, T. Lu, *Theranostics* **2020**, *10*, 9843; c) W. Wei, Y. Ma, X. Yao, W. Zhou, X. Wang, C. Li, J. Lin, Q. He, S. Leptihn, H. Ouyang, *Bioact. Mater.* **2021**, *6*, 998.
- [4] L. Bolano, J. A. Kopta, *Orthopedics* **1991**, *14*, 987.
- [5] a) J. E. Woodell-May, S. D. Sommerfeld, *J. Orthop. Res.* **2020**, *38*, 253; b) B. Arzi, G. DuRaine, C. Lee, D. Huey, D. Borjesson, B. Murphy, J. Hu, N. Baumgarth, K. Athanasiou, *Acta Biomater.* **2015**, *23*, 72; c) J. Malejczyk, A. Osiecka, A. Hyc, S. Moskalewski, *Clin. Orthop. Relat. Res.* **1991**, *269*, 266.
- [6] J. M. Anderson, A. Rodriguez, D. T. Chang, presented at *seminars in immunology*, Academic Press, **2008**, *20*. <https://doi.org/10.1016/j.smim.2007.11.004>
- [7] K. Flégeau, A. Puiggali-Jou, M. Zenobi-Wong, *Biofabrication* **2022**, *14*, 034105.
- [8] N. Fahy, E. Farrell, T. Ritter, A. E. Ryan, J. M. Murphy, *Tissue Eng., Part B* **2015**, *21*, 55.
- [9] L. Zhang, Z. Cao, T. Bai, L. Carr, J.-R. Ella-Menye, C. Irvin, B. D. Ratner, S. Jiang, *Nat. Biotechnol.* **2013**, *31*, 553.
- [10] S. Jiang, Z. Cao, *Adv. Mater.* **2010**, *22*, 920.
- [11] a) D. Dong, C. Tsao, H.-C. Hung, F. Yao, C. Tang, L. Niu, J. Ma, J. MacArthur, A. Sinclair, K. Wu, *Sci. Adv.* **2021**, *7*, 5442; b) Q. Liu, A. Chiu, L. Wang, D. An, W. Li, E. Y. Chen, Y. Zhang, Y. Pardo, S. P. McDonough, L. Liu, *Biomaterials* **2020**, *230*, 119640; c) Q. Liu, A. Chiu, L.-H. Wang, D. An, M. Zhong, A. M. Smink, B. J. de Haan, P. de Vos, K. Keane, A. Vegge, *Nat. Commun.* **2019**, *10*, 5262.
- [12] T. Bai, F. Sun, L. Zhang, A. Sinclair, S. Liu, J. R. Ella-Menye, Y. Zheng, S. Jiang, *Angew. Chem.* **2014**, *126*, 12943.
- [13] T. Bai, J. Li, A. Sinclair, S. Imren, F. Merriam, F. Sun, M. B. O'Kelly, C. Nourigat, P. Jain, J. J. Delrow, *Nat. Med.* **2019**, *25*, 1566.
- [14] a) P. E. Milner, M. Parkes, J. L. Puetzer, R. Chapman, M. M. Stevens, P. Cann, J. R. Jeffers, *Acta Biomater.* **2018**, *65*, 102; b) Z. Wang, J. Li, Y. Liu, J. Luo, *Tribol. Int.* **2020**, *143*, 106026; c) A. O. Osaheni, E. B. Finkelstein, P. T. Mather, M. M. Blum, *Acta Biomater.* **2016**, *46*, 245; d) Z. Wang, J. Li, L. Jiang, S. Xiao, Y. Liu, J. Luo, *Langmuir* **2019**, *35*, 11452.
- [15] a) J. Yang, Y. Han, J. Lin, Y. Zhu, F. Wang, L. Deng, H. Zhang, X. Xu, W. Cui, *Small* **2020**, *16*, 2004519; b) Y. Han, J. Yang, W. Zhao, H. Wang, Y. Sun, Y. Chen, J. Luo, L. Deng, X. Xu, W. Cui, *Bioact. Mater.* **2021**, *6*, 3596; c) H. Chen, T. Sun, Y. Yan, X. Ji, Y. Sun, X. Zhao, J. Qi, W. Cui, L. Deng, H. Zhang, *Biomaterials* **2020**, *242*, 119931; d) R. Xie, H. Yao, A. S. Mao, Y. Zhu, D. Qi, Y. Jia, M. Gao, Y. Chen, L. Wang, D.-A. Wang, *Nat. Biomed. Eng.* **2021**, *5*, 1189.
- [16] A. C. Daly, L. Riley, T. Segura, J. A. Burdick, *Nat. Rev. Mater.* **2020**, *5*, 20.
- [17] a) Q. Feng, D. Li, Q. Li, X. Cao, H. Dong, *Bioact. Mater.* **2022**, *9*, 105; b) T. P. Nguyen, F. Li, S. Shrestha, R. S. Tuan, H. Thissen, J. S. Forsythe, J. E. Frith, *Biomaterials* **2021**, *279*, 121214; c) F. Li, C. Levinson, V. X. Truong, L. A. Laurent-Applegate, K. Maniura-Weber, H. Thissen, J. S. Forsythe, M. Zenobi-Wong, J. E. Frith, *Biomater. Sci.* **2020**, *8*, 1711.
- [18] a) E. Sideris, D. R. Griffin, Y. Ding, S. Li, W. M. Weaver, D. Di Carlo, T. Hsiai, T. Segura, *ACS Biomater. Sci. Eng.* **2016**, *2*, 2034; b) A. Sheikhi, J. de Rutte, R. Haghniaz, O. Akouissi, A. Sohrabi, D. Di Carlo, A. Khademhosseini, *Biomaterials* **2019**, *192*, 560; c) A. Puiggali-Jou, M. Asadikorayem, K. Maniura-Weber, M. Zenobi-Wong, *Acta Biomater.* **2023**, *166*, 69.
- [19] a) Z. Luo, J. Pan, Y. Sun, S. Zhang, Y. Yang, H. Liu, Y. Li, X. Xu, Y. Sui, S. Wei, *Adv. Funct. Mater.* **2018**, *28*, 1804335; b) Y. Wang, X. Yuan, K. Yu, H. Meng, Y. Zheng, J. Peng, S. Lu, X. Liu, Y. Xie, K. Qiao, *Biomaterials* **2018**, *171*, 118; c) H. Yin, Y. Wang, X. Sun, G. Cui, Z. Sun, P. Chen, Y. Xu, X. Yuan, H. Meng, W. Xu, *Acta Biomater.* **2018**, *77*, 127; d) C. Erickson, M. Stager, M. Riederer, K. A. Payne, M. Krebs, *J. Biomater. Appl.* **2021**, *36*, 289; e) Q. Feng, Q. Li, H. Wen, J. Chen, M. Liang, H. Huang, D. Lan, H. Dong, X. Cao, *Adv. Funct. Mater.* **2019**, *29*, 1906690.
- [20] A. Sinclair, M. B. O'Kelly, T. Bai, H. C. Hung, P. Jain, S. Jiang, *Adv. Mater.* **2018**, *30*, 1803087.
- [21] L. G. Villa-Diaz, H. Nandivada, J. Ding, N. C. Nogueira-de-Souza, P. H. Krebsbach, K. S. O'shea, J. Lahann, G. D. Smith, *Nat. Biotechnol.* **2010**, *28*, 581.
- [22] D. Yang, J. Xiao, B. Wang, L. Li, X. Kong, J. Liao, *Mater. Sci. Eng., C* **2019**, *104*, 109927.
- [23] F. Wei, S. Liu, M. Chen, G. Tian, K. Zha, Z. Yang, S. Jiang, M. Li, X. Sui, Z. Chen, *Front. bioeng. biotechnol.* **2021**, *9*, 664592.
- [24] W. Zhao, Y. Zhu, J. Zhang, T. Xu, Q. Li, H. Guo, J. Zhang, C. Lin, L. Zhang, *J. Mater. Sci.* **2018**, *53*, 13813.
- [25] Z. Zhang, S. Chen, S. Jiang, *Biomacromolecules* **2006**, *7*, 3311.
- [26] a) V. Gaberc-Porekar, I. Zore, B. Podobnik, V. Menart, *Curr. Opin Drug Discovery Dev* **2008**, *11*, 242; b) G. T. Kozma, T. Shimizu, T. Ishida, J. Szebeni, *Adv. Drug Delivery Rev.* **2020**, *154*, 163; c) D. A. Herold, K. Keil, D. E. Bruns, *Biochem. Pharmacol.* **1989**, *38*, 73.
- [27] S. Xiao, T. Zhao, J. Wang, C. Wang, J. Du, L. Ying, J. Lin, C. Zhang, W. Hu, L. Wang, *Stem Cell Rev. Rep.* **2019**, *15*, 664.
- [28] A. E. Widener, S. Duraivel, T. E. Angelini, E. A. Phelps, *Adv. Nanobiomed. Res.* **2022**, *2*, 2200030.
- [29] A. J. Seymour, S. Shin, S. C. Heilshorn, *Adv. Healthcare Mater.* **2021**, *10*, 2100644.

- [30] a) A. C. Sutarin, A. J. Krüger, K. Neidig, N. Klos, N. Dolfen, M. Bund, T. Gronemann, R. Sebers, A. Manukanc, G. Yazdani, *Adv. Healthcare Mater.* **2022**, *11*, 2200989; b) D. L. Braunmiller, S. Babu, D. B. Gehlen, M. Seuß, T. Haraszti, A. Falkenstein, J. Eigen, L. De Laporte, J. J. Crassous, *Adv. Funct. Mater.* **2022**, *32*, 2202430.
- [31] a) T. H. Qazi, J. Wu, V. G. Muir, S. Weintraub, S. E. Gullbrand, D. Lee, D. Issadore, J. A. Burdick, *Adv. Mater.* **2022**, *34*, 2109194; b) J. Wu, S. Yadavali, D. A. Issadore, D. Lee, *Adv. Mater. Technol.* **2022**, *7*, 2101160; c) C. W. Visser, T. Kamperman, L. P. Karbaat, D. Lohse, M. Karperien, *Sci. Adv.* **2018**, *4*, 1175.
- [32] A. C. Daly, *Adv. Healthcare Mater.* **2023**, 2301388. <https://doi.org/10.1002/adhm.202301388>
- [33] B. Kessel, M. Lee, A. Bonato, Y. Tinguely, E. Tosoratti, M. Zenobi-Wong, *Adv. Sci.* **2020**, *7*, 2001419.
- [34] V. G. Muir, T. H. Qazi, J. Shan, J. r. Groll, J. A. Burdick, *ACS Biomater. Sci. Eng.* **2021**, *7*, 4269.
- [35] A. S. Caldwell, V. V. Rao, A. C. Golden, K. S. Anseth, *Biomaterials* **2020**, *232*, 119725.
- [36] S. Uman, A. Dhand, J. A. Burdick, *J. Appl. Polym. Sci.* **2020**, *137*, 48668.
- [37] B. D. Olsen, J. A. Kornfield, D. A. Tirrell, *Macromolecules* **2010**, *43*, 9094.
- [38] E. Cavalli, C. Levinson, M. Hertl, N. Brogiere, O. Brück, S. Mustjoki, A. Gerstenberg, D. Weber, G. Salzmänn, M. Steinwachs, *Sci. Rep.* **2019**, *9*, 4275.
- [39] a) M. Sato, M. Yamato, G. Mitani, T. Takagaki, K. Hamahashi, Y. Nakamura, M. Ishihara, R. Matoba, H. Kobayashi, T. Okano, *npj Regener. Med.* **2019**, *4*, 4; b) H. Adkisson, C. Milliman, X. Zhang, K. Mauch, R. Maziarz, P. Streeter, *Stem Cell Res.* **2010**, *4*, 57; c) P. Smeriglio, J. H. Lai, L. Dhulipala, A. W. Behn, S. B. Goodman, R. L. Smith, W. J. Maloney, F. Yang, N. Bhutani, *Tissue Eng., Part A* **2015**, *21*, 147.
- [40] Y. Chang, S.-C. Liao, A. Higuchi, R.-C. Ruaan, C.-W. Chu, W.-Y. Chen, *Langmuir* **2008**, *24*, 5453.
- [41] Ø. Arlov, D. Rüttsche, M. Asadi Korayem, E. Öztürk, M. Zenobi-Wong, *Adv. Funct. Mater.* **2021**, *31*, 2010732.
- [42] J. Wu, Z. Xiao, A. Chen, H. He, C. He, X. Shuai, X. Li, S. Chen, Y. Zhang, B. Ren, *Acta Biomater.* **2018**, *71*, 293.
- [43] B. A. Aguado, W. Mulyasasmita, J. Su, K. J. Lampe, S. C. Heilshorn, *Tissue Eng., Part A* **2012**, *18*, 806.
- [44] a) P. Fisch, N. Brogiere, S. Finkelsztejn, T. Linder, M. Zenobi-Wong, *Adv. Funct. Mater.* **2021**, *31*, 2008261; b) A. Bonato, P. Fisch, S. Ponta, D. Fercher, M. Manninen, D. Weber, K. K. Eklund, G. Barreto, M. Zenobi-Wong, *Adv. Healthcare Mater.* **2023**, 2202271 <https://doi.org/10.1002/adhm.202202271>; c) R. Levato, W. R. Webb, I. A. Otto, A. Mensinga, Y. Zhang, M. van Rijen, R. van Weeren, I. M. Khan, J. Malda, *Acta Biomater.* **2017**, *61*, 41.
- [45] C. Rodriguez-Emmenegger, M. Houska, A. B. Alles, E. Brynda, *Macromol. Biosci.* **2012**, *12*, 1413.
- [46] Y. Wu, Q. Lai, S. Lai, J. Wu, W. Wang, Z. Yuan, *Colloids Surf., B* **2014**, *118*, 298.